Photochemical and Molecular Dynamics Studies of Halide Binding in Flavoenzyme Glucose Oxidase

Bo Zhuang, Marten Vos, Alexey Aleksandrov

RESEARCH ARTICLE

Photochemical and Molecular Dynamics Studies of Halide Binding in Flavoenzyme Glucose Oxidase

Bo Zhuang, Marten H. Vos,* Alexey Aleksandrov*

B. Zhuang, Dr. M. H. Vos, Dr. A. Aleksandrov
LOB, CNRS, INSERM
École Polytechnique, Institut Polytechnique de Paris
91128 Palaiseau, France
E-mail: marten.vos@polytechnique.edu (M. H. V.), alexey.aleksandrov@polytechnique.edu (A. A.)

Supporting information for this article is given via a link at the end of the document.

Abstract: Glucose oxidase (GOX), a characteristic flavoprotein oxidase with widespread industrial applications, binds fluoride (F^-) and chloride (Cl^-). We investigated binding properties of halide inhibitors of GOX through time-resolved spectral characterization of flavin-related photochemical processes and molecular dynamic simulations. Cl^- and F^- bind differently to the protein active site and have substantial but opposite effects on the population and decay of the flavin excited state. Cl^- binds closer to the flavin, whose excited-state decays in <100 fs due to anion–π interactions. Such interactions appear absent in F^- binding, which, however, significantly increases the active-site rigidity leading to more homogeneous, picosecond fluorescence decay kinetics. These findings are discussed in relation to the mechanism of halide inhibition of GOX by occupying the accommodation site of catalytic intermediates and increasing the active-site rigidity.

Introduction

Flavoprotein oxidases catalyze the oxidation of substrates by dioxygen (O_2).[1,2] Their reaction cycles can be divided in the reductive half-cycle, in which a substrate is oxidized by transfer of two electrons and two protons to the flavin cofactor of the enzyme followed by the release of the first product, and an oxidative half-cycle in which the resting oxidized flavin is recovered by electron transfer (ET) to the second substrate O_2. The latter half-reaction occurs mainly in two steps.[3,4] The first step is the oxidation of flavin hydroquinone by O_2 to generate flavin semiquinone and superoxide radical anion ($O_2^{\bullet-}$). During the second step, the second product, hydrogen peroxide (H_2O_2) is generated, either by the transfer of a second electron from the flavin semiquinone to $O_2^{\bullet-}$, or sometimes via the formation and decomposition of a flavin-C4a-hydroperoxide intermediate, and the flavin returns to its resting oxidized state.[3] In flavin-dependent enzymes, O_2 reduction usually exhibits rate enhancements by 3−4 orders of magnitude compared with the reactions between free flavin hydroquinones and O_2 in solution.[4,5] It has been proposed that positive charges in the active site of flavoprotein oxidases constitute a preorganized anion-binding site that electrostatically stabilizes the $O_2^{\bullet-}$ intermediate, thus activating O_2 for reaction with flavin hydroquinone.[4–9] Halide ions have been used as surrogates for oxygen species in the study of oxygen activation in several enzymes.[9–13] Among them, glucose oxidase (GOX) from *Aspergillus niger*, an acid-tolerant fungus,[14] is a popular flavoprotein model that has widespread applications in pharmaceutical, food, and beverage chemistry, and biotechnology.[15] GOX harbors a flavin adenine dinucleotide (FAD) cofactor and physiologically catalyzes the oxidation of β-D-glucose to glucono-δ-lactone by O_2, operating by a ping-pong bi-bi mechanism, with oxidized FAD (FAD_{ox}) being the functional resting state.[16] It is stable across a wide pH range, more active at acidic conditions and preserves very high activity at pH as low as 3.0.[17] This robustness also contributes to the versatility of its applications. The sugar and O_2 substrates of GOX, that bind in the reductive and oxidative half-cycles respectively, are thought to occupy partly overlapping binding sites.[9,16,18] It has long been known that halide ions can inhibit the enzyme[17,19] and alter its redox potentials,[20] although the underlying mechanisms are not yet clear. A previous study has used chloride (Cl^-) as a mimic for $O_2^{\bullet-}$ to probe the oxygen activation site in GOX, demonstrating the specific binding of Cl^- by its alteration of the FAD_{ox} absorption spectrum, as well as the involvement of a titratable residue (suggested to be His516) in halide binding.[9] The detailed characteristics at the molecular level of the accommodation of Cl^- in the active site are still rather elusive due to the lack of a crystal structure of GOX complexed with Cl^-.

In general, time-resolved spectral characterization of flavin-related photochemical processes, and in particular flavin photoreduction and re-oxidation cycles, can be employed as a probe for the active-site configurations and dynamics in flavoproteins, as the kinetics and intermediates of such processes are very sensitive to the immediate flavin environment.[21–27] In most cases, binding of halide ions can induce significant conformational changes in proteins.[28–30] For flavoproteins, in addition to spectral shifts due to an altered electrostatic environment, the presence of halide ions near the flavin cofactor may also result in anion–π interactions with a charge-transfer (CT) component in the ground state, thus directly affecting the electronic structure of the isoalloxazine ring system itself.[31,32] Altogether, we hypothesized that investigating photochemical processes in flavoprotein–halide complexes using ultrafast spectroscopy can provide useful insight into the anion-binding properties of the proteins. In the present work, we report the effects of fluoride (F^-) and Cl^- binding on the decay of the excited singlet FAD_{ox} cofactor ($^SFAD^*$) and the formation of photoproducts in GOX. In time-resolved fluorescence and transient absorption measurements, we observed substantial, but unexpectedly opposite, effects of F^- and Cl^- binding on the photochemistry of GOX. Using molecular dynamics (MD) simulations, we modeled the binding process of the halides to the protein, which not only provided assessments of the anion-binding sites, but also allowed

the experimental findings to be related to atomistic details, including an increase of active-site rigidity upon F^- binding, and closer interactions between FAD_{ox} and Cl^-. This work illustrates the molecular basis of F^- and Cl^- binding in GOX and helps to understand the mechanism of halide inhibition in this important flavoprotein oxidase.

Results and Discussion

Binding of halides

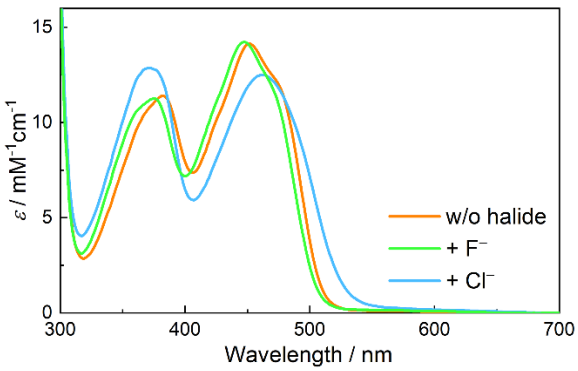

Figure 1. Steady-steady absorption spectra of GOX in the absence of halides, with 50 mM KF or 100 mM KCl at pH 3.0.

The binding of F^- or Cl^- alters the steady-state absorption spectrum of FAD_{ox} in GOX, and the spectra obtained in the presence of a large excess of F^- or Cl^- at pH 3.0 are shown in Figure 1. As reported in Ref. [9], binding of Cl^- strongly perturbs the spectrum of FAD_{ox}. The lowest transition band of FAD_{ox} at ~450 nm is red-shifted by ~30 nm (at the red edge), and the near-ultraviolet band is blue-shifted by ~10 nm (at the maximum). Remarkably, the relative intensities of these two bands are inversed, which is seldom observed for protein-bound FAD_{ox}, and the vibrational structure of the spectrum disappears. On the other hand, the formation of the GOX:F^- complex causes smaller changes to the FAD_{ox} absorption: for both bands in the near-ultraviolet/visible range only hypsochromic shifts of a few nanometers. Notably, the ~450-nm bands of F^- and Cl^- binding samples shift in opposite directions. The steady-state fluorescence emission spectra (Figure S1, Table S2) also show that F^- and Cl^- binding have different effects on the fluorescence intensity and emission maximum of GOX. It should be noted that this integrated fluorescence is expected to include substantial contributions from any trace amounts of free flavin (*vide infra*).

As flavin dissociation can lead to an increase in fluorescence intensity, to investigate the possibility that F^- binding enhances the concentration of free flavin, we examined the amount of free flavin in the sample containing excess F^-. By comparing with that in the sample with no F^- added, we assessed that under our experimental conditions F^- binding itself does not induce any noticeable flavin dissociation (Figure S2).

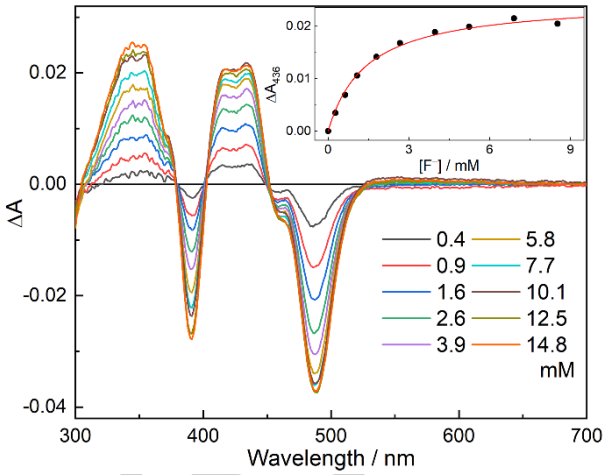

Figure 2. Difference spectra obtained during the titration process of GOX with KF in 50 mM potassium citrate buffer at pH 3.5. The inset shows a plot of absorbance changes at 436 nm as a function of the concentrations of F^-. The solid red line in the inset was obtained by fitting a theoretical binding curve according to eq 1.

The K_d for the GOX:Cl^- complex has been determined in the literature by spectral titration of GOX with Cl^-.[9,19] The corresponding experiment on F^- binding is lacking. We therefore performed titrations of GOX with KF for pH of 3.0, 3.5 and 4.0. Difference spectra exhibit broad positive bands centered at ~345 and ~428 nm and prominent negative peaks at 390 and 488 nm and do not change in shape during the titration (Figure 2). The K_d for the GOX:F^- complex was calculated by analysis of the observed increase in absorbance at the 436 nm maximum (the inset of Figure 2, Figure S3, Table S1). Over the pH range investigated, the titrations show that the GOX:F^- complex has a smaller K_d compared with that of the GOX:Cl^- complex (e.g., 0.28 mM and 6.20 mM, respectively, at pH 3.0; cf. Ref. [9]), consistent with the fact that F^- is a much more effective inhibitor of GOX than Cl^-.[17] Similar to the GOX:Cl^- complex, in this range the K_d for the GOX:F^- complex rises with pH, suggesting that the same titratable residue may be responsible for both Cl^- and F^- binding, which has been assigned to His516 in the previous study.[9]

Time-resolved spectral characterization

The changes in the steady-state absorption spectrum of GOX indicate that both F^- and Cl^- very likely bind close to the FAD_{ox} cofactor, yet presumably in different manners. They are thus expected to influence the active-site environment and therewith the photophysical and photochemical properties of FAD_{ox}. To further investigate the anion-binding sites in GOX, we performed time-resolved fluorescence and transient absorption measurements on the GOX–halide complexes. The photochemistry of GOX in the absence of halides is relatively well-understood. Upon excitation of FAD_{ox} in GOX, the flavin fluorescence is effectively quenched by photoinduced ET from close-by tyrosines (TyrOH) to $^SFAD^*$ in a few picoseconds;[33–35] the resulting $FAD^{\bullet-}$/$TyrOH^{\bullet+}$ radical pairs subsequently recombine, either directly or following further ET and proton transfer processes.[35]

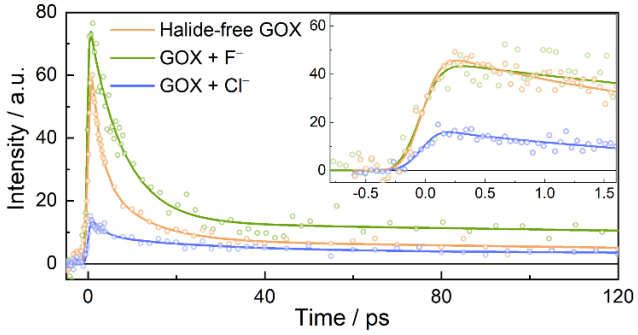

Figure 3. Fluorescence decays of the halide-free and halide-binding GOX samples monitored at 534 nm, with CS_2 or suprasil (inset) as Kerr medium. Intensities were normalized based on the absorption of the samples at the excitation wavelength (390 nm).

The experiments were performed at pH 3.0, where halide anions easily bind (*vide supra*).[17] As shown in Figure 3, Figure S4, and summarized in Table S2, the fluorescence decay of the halide-free sample of GOX is multiphasic and can be fitted with time constants of 2 ps (62%) and 10 ps (29%), as well as a small long-lived component (9%) that is most likely due to some free flavin present at this low pH (Figure S2). The kinetics are modestly slower than those reported for GOX at neutral pH (fitted with time constants of 1 and 4 ps[35]) indicating that pH has an effect on the configurations of the FAD_{ox}–TyrOH pairs, presumably due to the rearrangement of the hydrogen bonding network in the active site. Similar to that at neutral pH, the multiphasic fluorescence decay here is ascribable to the involvement of conformational heterogeneity of the active site.[35] Upon the binding of F^-, the 2-ps and 10-ps fluorescence decay phases (from the halide free experiment) merge to a single 7-ps phase (89%), leading to an overall slower decay. A possible interpretation here is that the binding of F^- increases the rigidity of the active site, and hence reduces conformational heterogeneity of the electron donor–acceptor pairs.

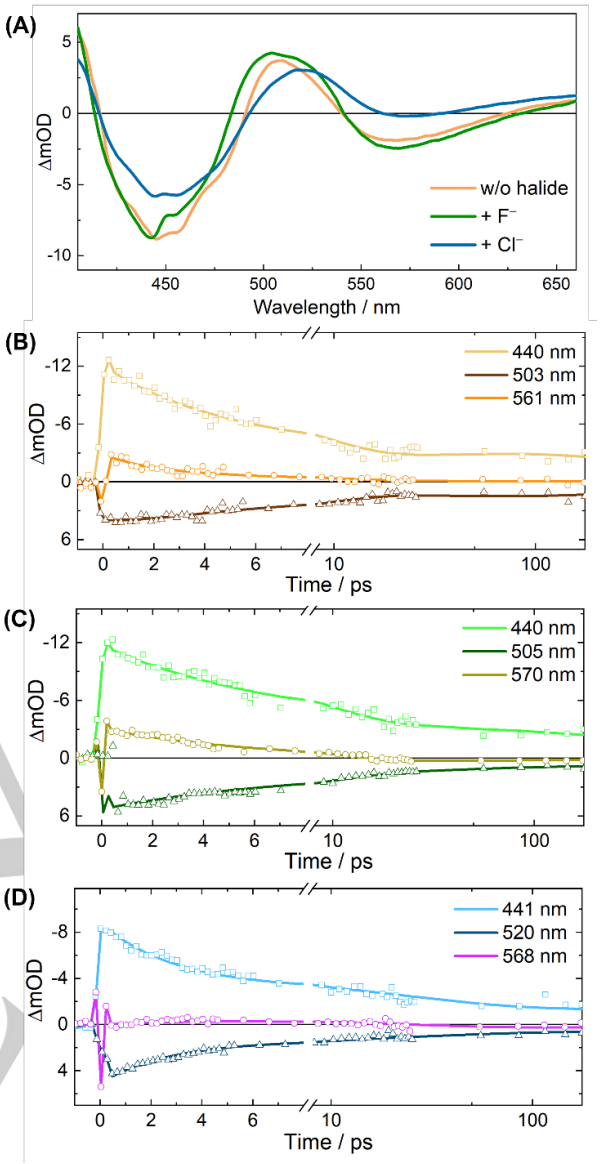

Figure 4. Isotropic transient absorption spectra of the GOX samples measured at 3 ps after excitation (A), as well as the kinetic traces of the halide-free (B), F^--binding (C) and Cl^--binding (D) GOX at selected wavelengths. The time axis of the kinetic trances is linear up to 8 ps and logarithmic thereafter.

The binding of Cl^- has a very different effect on the fluorescence kinetics (Figure 3). The observed initial amplitude of the fluorescence is much lower, including at the highest time resolution available (Figure 3, inset), where it is ~64% lower. Assuming the intrinsic initial fluorescence intensity is unchanged, this would imply a very fast initial fluorescence decay on a timescale much shorter than the instrument response; we estimate < 100 fs. Yet, ultrafast fluorescence decay in less than 100 fs by intermolecular ET from nearby redox-active residues is highly unexpected for protein-bound FAD_{ox}, suggesting that for the majority of GOX:Cl^- complexes a different quenching mechanism may be involved (*vide infra*). Phases of 3 ps and 27 ps (amplitudes of ~17% and ~9% with respect to the initial amplitude observed in the absence of Cl^-, respectively) are also required to fit the data, suggesting conformational heterogeneity,

possibly including contributions from GOX devoid of Cl^-. A small long-lived phase similar to the halide-free sample was also observed for the F^- and Cl^- containing samples (Table S2), which is assignable to a small amount of free flavin.

As fluorescence decays only provide information on excited-state kinetics, to visualize the photoproducts, we performed transient absorption measurements on halide-free, F^-- and Cl^--binding GOX. The full data are shown as false-color maps in Figure S5, and the transient spectra measured 3 ps after excitation, as well as kinetic traces at selected wavelengths, are shown in Figure 4. The evolution of the spectra is clearly wavelength dependent. For all three samples, the negative band around 450 nm that is dominated by ground-state bleaching, as well as the induced absorption bands below 415 nm, around 510 nm, and beyond 620 nm, were consistently observed. The induced band at ~510 nm of the GOX:Cl^- complex, however, is notably red-shifted compared with that of the other two. Another pronounced negative band around 565 nm, which reflects stimulated emission from the excited state, was observed for the halide-free and F^--binding GOX as well (Figure 4A, B and C), but for the GOX:Cl^- complex it is strikingly weak (Figure 4A, D), in agreement with the low initial amplitude in the time-resolved fluorescence experiments (Figure 3).

Multi-exponential global analysis of these transient absorption data was carried out. The found time constants were mostly very similar to those from the analysis of the time-resolved fluorescence experiments. The results are further depicted in terms of evolution associated spectra (EAS), which correspond to spectra of intermediate states assuming a linear sequential reaction scheme. The EAS of the product states are given in Figure 5. The 2-ps phase EAS of halide-free GOX and the 7-ps phases EAS of the GOX:F^- complex have the characteristic spectral features of $^{S}FAD^*$, including pronounced stimulated emission bands, thus representing the dominant initial excited-state decay due to ET from close-by tyrosines, in accordance with the time-resolved fluorescence results (Table S2). The slightly red-extended bleaching feature of the halide-free GOX compared with that of the GOX:F^- complex also corresponds well with their steady-state absorption spectra (Figure 1). In halide-free GOX at pH 3.0, the spectral evolution after the formation of $^{S}FAD^*$ is complex, with multiphasic $^{S}FAD^*$ decay partly taking place on similar timescales as the evolution of the product state involving charge recombination, flavin protonation, and further ET (Figure 5A), in a qualitatively similar way as at pH 8.0.[35] For instance, the 8-ps phase EAS of halide-free GOX arises from $^{S}FAD^*$ absorption and stimulated emission, as well as of a fraction of the $FAD^{\bullet-}$/$TyrOH^{\bullet+}$ product state that decays on this timescale.

For the GOX:F^- complex, the dominant phase is the 7-ps phase, which has the characteristics of $^{S}FAD^*$ (Figure 5B). The much lower amplitude of the longer-lived phases indicates that the presumed $FAD^{\bullet-}$/$TyrOH^{\bullet+}$ product state decays on a timescale much faster than 7 ps, predominantly by charge recombination, and partly by radical pair stabilization processes (cf. Ref. [35]). The involved photochemical reactions upon the excitation of halide-free and F^--binding GOX are summarized in a simplified way in Scheme 1.

On the other hand, the 3-ps phase EAS of Cl^- binding GOX hardly displays any stimulated emission feature (Figure 5C). Along with the fact that as deduced from the time-resolved fluorescence measurements (*vide supra*), a non-fluorescent ("dark") product state can form in less than 100 fs, and only ~17% of the fluorescence decays with a similar lifetime (4 ps), we propose that the 3-ps phase EAS is essentially dominated by this product state. A CT-type mechanism has been proposed to explain the quenching of flavin fluorescence by halides.[36] Considering the quasi-instantaneous appearance of the dark state, a CT excitation of the [FAD_{ox}···Cl^-] complex that gives rise to the direct formation of a transient state with [$FAD^{\bullet-}$···$Cl^{\bullet}$] character (spin inversion within this intermediate pair may lead to direct reformation of the ground state rather than the formation of long-lived free radicals [36]) is the most likely explanation. Such direct CT excitation can be enabled by strong interactions between the donor–acceptor pair to provide reasonable oscillator strength.[37] We note that anion–π interactions have been reported to contribute to an important binding mode occurring between halides and flavoproteins.[31,32]

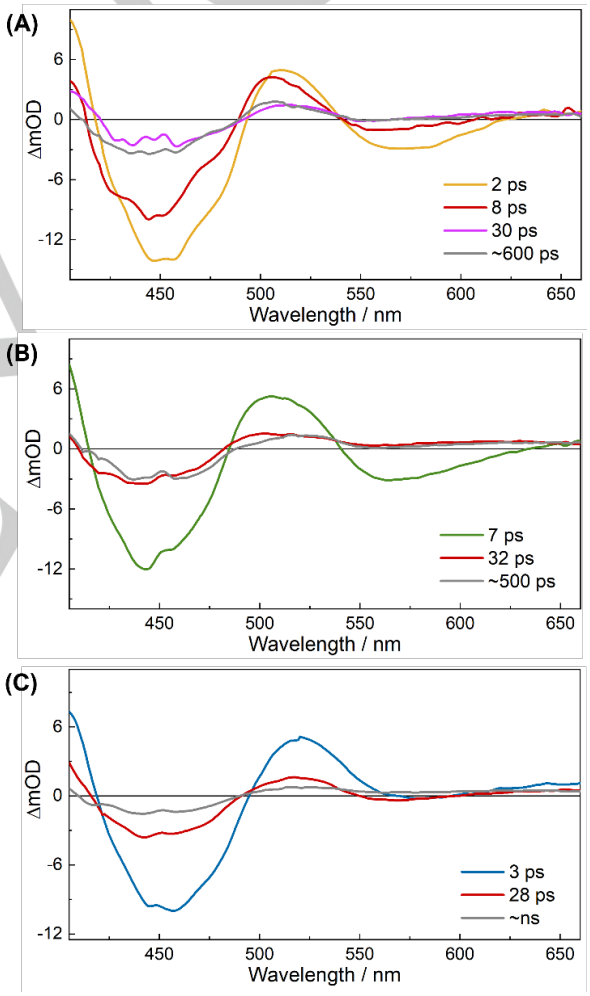

Figure 5. EAS from the global analysis of transient absorption data of halide-free (A), F^--binding (B) and Cl^--binding (C) GOX.

The existence of anion–π interactions in the GOX:Cl^- complex is implied by the red-extended steady-state absorption of Cl^- binding GOX, which may constitute an overlapping CT component (Figure 1),[38] as well as the red-shifted transient spectrum of $FAD^{\bullet-}$ in the 3-ps spectrum (Figure 4A).[26] Furthermore, anion–π interactions have been shown to regulate the redox potential of the flavin cofactor[39] and a dependency of

the reduction mechanism of GOX and the redox potential on the presence of Cl^- was indeed observed.[20] As illustrated in Scheme 2, we note that with the current measurements we cannot fully exclude the possibility that the CT state with [$FAD^{\bullet-}\cdots Cl^{\bullet}$] character is not directly accessed but through nonadiabatic transition from a higher-lying local excited (LE) state,[40] which, nevertheless, also requires strong interactions between FAD_{ox} and Cl^- in the ground state.

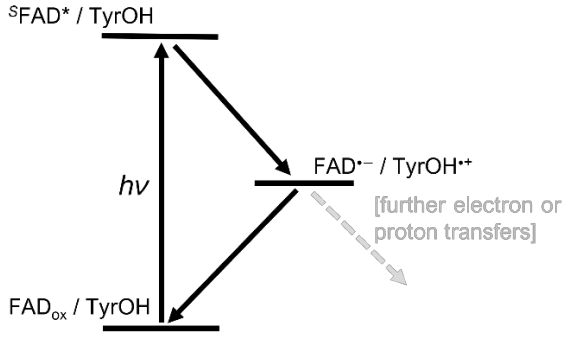

Scheme 1. Proposed minimal reaction scheme of photochemical processes of halide-free and F^- binding GOX.

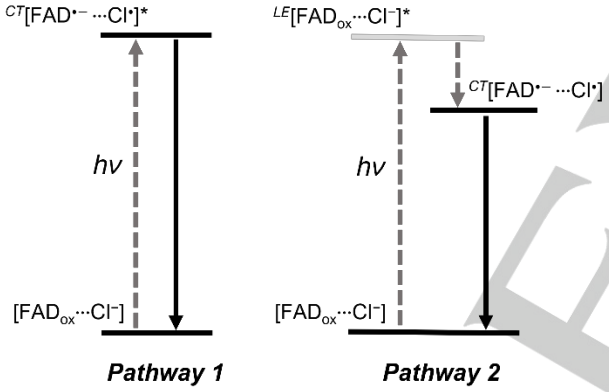

Scheme 2. Proposed two possible pathways to access the CT state upon the excitation of Cl^- binding GOX.

Structural dynamics probed by MD simulations

To help interpret the *a priori* unexpected experimental findings and obtain detailed insights into the anion-binding properties of GOX, we performed all-atom MD simulations with classical force fields (henceforth referred to as "MD simulations") to model the binding processes of the halides. Four independent 100-ns runs with random initial positions of either F^- or Cl^- (corresponding to the ~100 mM concentration) were performed. Importantly, these simulations were initiated with halides occupying positions outside the protein system with the active site filled by water. MD simulations of the protein system in the absence of the halides were also carried out for comparison. Figure S6 shows the root-mean-square deviation (RMSD) for the protein backbone, indicating that all the systems are stable during the 100-ns trajectories. Dynamics of the distances between any non-hydrogen atoms of the flavin ring and the closest F^- or Cl^- in the simulations are shown in Figure S7. These demonstrate that both F^- and Cl^- diffuse into the active site of GOX and are observed in the vicinity of the FAD_{ox} cofactor. This exchange of halides between the protein and solution occurs on the nanosecond timescale or faster, suggesting that the length of MD simulations was appropriate in this study.

We then calculated the density maps that portray the resident sites of F^- and Cl^- over the course of 400-ns (4 independent simulations of 100 ns) simulations. As shown in Figure 6B, the density of Cl^- shows only one preferable binding site situated close to the flavin *re*-face, between protonated His516 and His559, which is occupied 94% of the time in the MD simulations, forming a well-defined flavin–chloride binary complex.

As the classical force fields used in the MD simulations did not take into account the effects of polarization, we conducted geometry optimizations on the flavin–chloride complex in GOX using a quantum mechanics/molecular mechanics (QM/MM) approach to investigate the interactions between FAD_{ox} and Cl^- in GOX at a higher level of theory, by further minimizing the geometry of one snapshot from the classical MD simulations to obtain a minimal structure, to evaluate whether the binding position revealed by MD simulations is sufficiently accurate. The QM/MM calculations were carried out with both the isoalloxazine ring structure and Cl^- included in the QM region, which was described by density functional theory (DFT). The results (Figure S8) show that in the flavin–chloride complex, substantial noncovalent interactions indeed are present between FAD_{ox} and Cl^-, which slightly deform the flavin ring; the position of Cl^- after the QM geometry optimization, nevertheless, is virtually identical to that from the MD simulations, demonstrating that in GOX, the noncovalent interactions between FAD_{ox} and Cl^- are not a major contributor to the Cl^- binding. This finding is further supported by QM-only (DFT) geometry optimization of the isolated flavin–chloride complex without the protein environment (Figure S9), which indicates that the present conformation of the flavin–chloride complex is not stable by itself, and needs protein residues. Altogether, the position of Cl^- binding site is largely determined by the steric constraints of and the electrostatic interactions with the protein moieties (mostly, His516 and His559), as demonstrated by MD simulations.

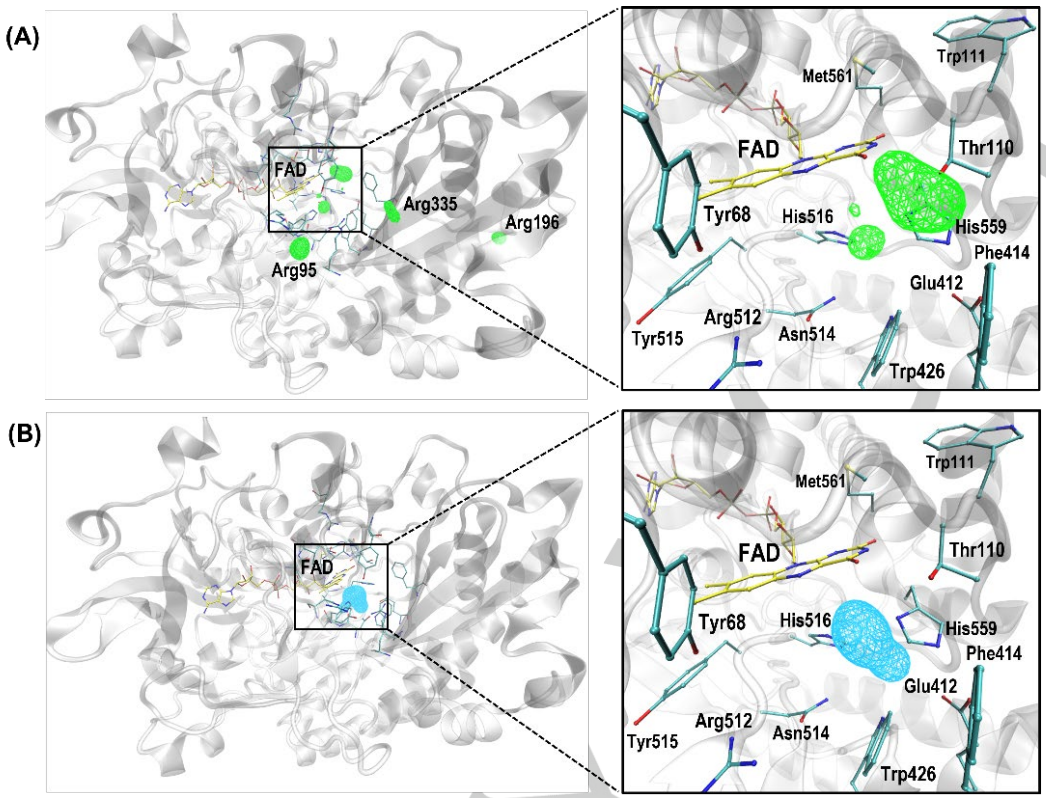

Figure 6. Density maps (colored mesh; isovalue: 0.24) of F^- (A) and Cl^- (B) extracted from the MD simulations, superimposed on the experimental crystal structure (PDB entry: 1CF3).

By contrast, F^- can reside at multiple distinct binding sites in the protein. At the sites remote from the active site containing the flavin cofactor, F^- interacts mostly with arginines (Figure 6A). In the protein active site, the dominant binding cavity is located between Thr110 and the O4 atom of FAD_{ox} (54%), whereas a position near His516 is accessible to F^- as well but with a lower relative occupancy (34%). Notably, during the MD simulations, in the vicinity of the active site these two binding sites were not filled by two F^- ions simultaneously, indicating that there is an equilibrium between the occupancies of these two sites and the total occupancy of the two sites is a simple sum of the two occupancies (88%) and near-quantitative. We further applied time-dependent DFT (TDDFT) calculations to investigate which of the two binding sites F^- is more likely to perturb the absorption spectrum of FAD_{ox} based on a simple point-charge model. The results (Figure S10 and Table S3) indicate that, whereas at both sites the presence of a negative point charge of e^- leads to blue shifts of the flavin absorption bands, the lowest transition is more affected when the negative charge is placed at the position corresponding to the binding site of F^- situated between Thr110 and the O4 atom of the flavin. Generally, we note that despite the simplicity of the model there is a very good agreement between the calculated and observed spectral shifts due to F^- binding: the shifts and amplitude changes of both bands are quantitatively similar (Figure 1). This observation further supports the binding model emerging from the MD simulations. The fact that the shape of the spectral changes remains unchanged during the entire F^- titration (Figure 2) indicates that the relative occupation of both sites near the flavin remains unchanged, in agreement with the one-site-binding-at-a-time model, as deduced from the simulations. From the unchanged relative occupation of both sites, we can also hypothesize that there is only one titratable residue (His516) that affects F^- binding, while other protein residues either do not titrate at the investigated pH range or are too distant to affect F^- binding.

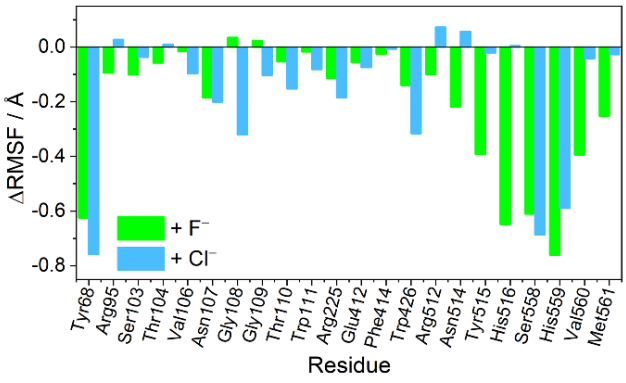

Figure 7. Difference RMSF of the Cα-atoms of active-site residues (within 10 Å of the flavin ring) in the MD simulations of GOX containing F^- or Cl^-, with respect to the halide-free simulations (see also Figure S11).

The root-mean-square fluctuations (RMSF) of the Cα-atoms for the simulations of halide-free GOX are given in Figure S11A. They are similar to those reported for the simulations of GOX at neutral pH,[18] showing that in GOX certain active-site residues, especially Tyr68, are highly flexible, in agreement with the reported B-factors of the crystal structure.[41] The RMSF difference, ΔRMSF, of the halide-containing simulations with respect to the halide-free simulations are given in Figure S11B, and C, where positive values denote increases and negative values denote decreases in residue flexibility induced by the halides. The results reveal that the presence of F^- and Cl^- gives rise to notable destabilization of *β*-sheet D (residues 77–81 and 93−97) and an adjacent loop (residues 82–92). However, in the protein active site, significant decreases in flexibility of almost all the residues that surround the FAD_{ox} cofactor were observed, among which Tyr68, Ser558, His559 and His516 are the most affected (Figure 7). This finding indicates that the incorporation of F^- and Cl^- leads to a more rigid active site. It appears that F^- has a larger influence on the increases in rigidity, as F^- is smaller in size and is a much stronger acceptor for hydrogen bonding and therefore can establish interactions with more residues in the active site than Cl^-. *β*-sheet D constitutes a part of the substrate-binding domain in GOX, and Tyr68, Thr110, Arg512, Asn514 and His559 were reported to be important in the accommodation of substrates in the active site.[41] Therefore, the changes in their flexibility may play a role in the inhibition of GOX by halides (where F^- is a more effective inhibitor), hindering the accommodation of the sugar substrates.

In the catalytic cycle of GOX, His516 is an important residue that has been described to participate in the concerted proton and hydride transfer in the reductive half-reaction,[16,18] and has been demonstrated to be responsible for the oxygen activation in the oxidative half-reaction.[6,16] The simulations of halide-free GOX show that His516 is relatively flexible (Figure S12A and S11A), consistent with previous computational studies.[18,42] During the F^-- and Cl^--containing simulations, both F^- and Cl^- interact with His516 when present in the GOX active site (Figure 6). The binding of F^- greatly reduces the flexibility of this residue (Figure 7 and S12B), which is also reflected in the analysis of the sidechain dihedrals, χ_1 and χ_2 (Figure 8 and S15). In the absence of a substrate and at a low pH, the dihedral angle χ_1 mainly adopts g^- geometry (~60°) with a small population of the *t* geometry (~±180°) (Figure 8A), which is diminished by the binding of F^- and Cl^- (Figure 8B, C). The χ_2 dihedral angle samples two broadly defined minima, Ng^+ (between −120° and 0°) and Ng^- (between 0° and 120°). It is worth noting that the binding of F^- significantly populates the (g^-, Ng^+) conformation (Figure 8B). It has been demonstrated that in the (g^-, Ng^+) conformation, His516 moves away from the sugar substrate, making the active site geometrically and chemically unfavorable for the concerted proton and hydride transfer in the reductive half-reaction.[18] This may also contribute to the F^- inhibition of GOX, by locking the His516 in a catalytically inactive conformation, which does not appear to be the case in Cl^--binding GOX.

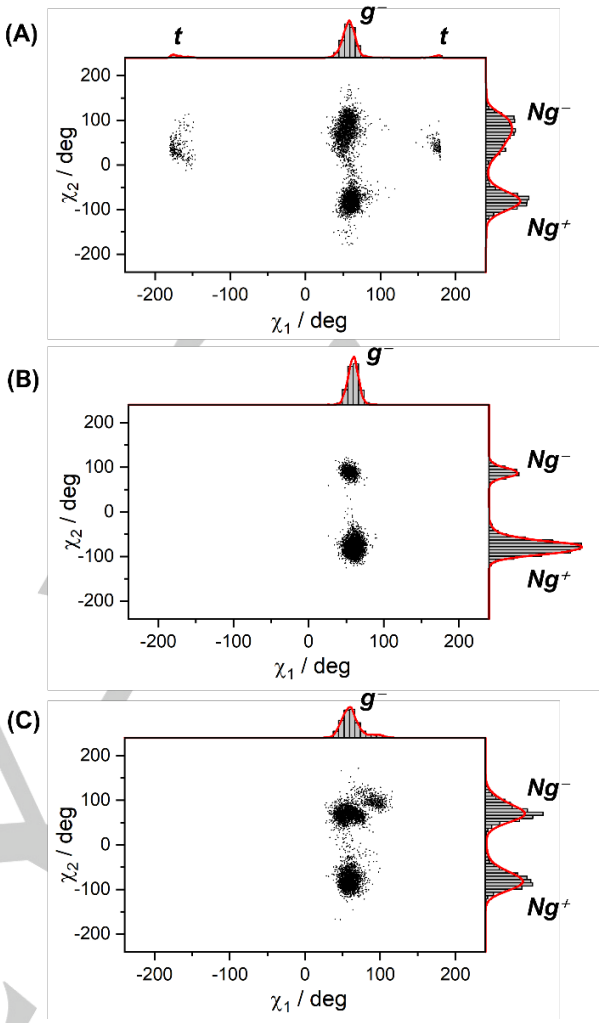

Figure 8. Dihedral angles (χ_1 and χ_2) distribution of the His516 side chain in the MD simulations of halide-free GOX (A), and the simulations containing F^- (B) and Cl^- (C). The distributions (histograms and normalized integrated curves) are shown on either side of the panels.

We will now discuss the results of the MD simulations with respect to our experimental observations using time-resolved fluorescence and transient absorption. Dynamics of the distances between FAD_{ox} and nearby electron-donating residues in the active site throughout 400-ns simulations are presented in Figure S13 and S14. Figure 9 shows the corresponding distance distributions between FAD_{ox} and the two primary electron-donating residues, Tyr68 and Tyr515 in the photochemistry of halide-free GOX.[35] Here, the minimal ring-to-ring distance is used, which is defined as the shortest distance between any non-hydrogen atoms from two rings and is thought to be relevant to the electronic coupling in ET reactions between two aromatic systems. As also demonstrated by RMSF (Figure S11A), Tyr68 is a highly flexible residue, which rationalizes the multiphasic fluorescence decay in the halide-free GOX. In the presence of F^- or Cl^-, during the simulations Tyr68 clearly exhibits less conformational heterogeneity compared with that of halide-free GOX (Figure 9A). Although the FAD_{ox}–Tyr515 distance distributions are less heterogeneous than the FAD_{ox}–Tyr68 pair,

in the presence of F^- the distribution (Figure 9B) appears to have a smaller standard deviation (SD: 0.22 Å), compared with that of the halide-free simulations (SD: 0.30 Å). Importantly, longer distances between FAD_{ox}–Tyr515 are less likely, as can be seen from the smaller positive skewness in the presence of F^- (1.0 and 0.4 for the halide-free and F^- containing simulations, respectively).

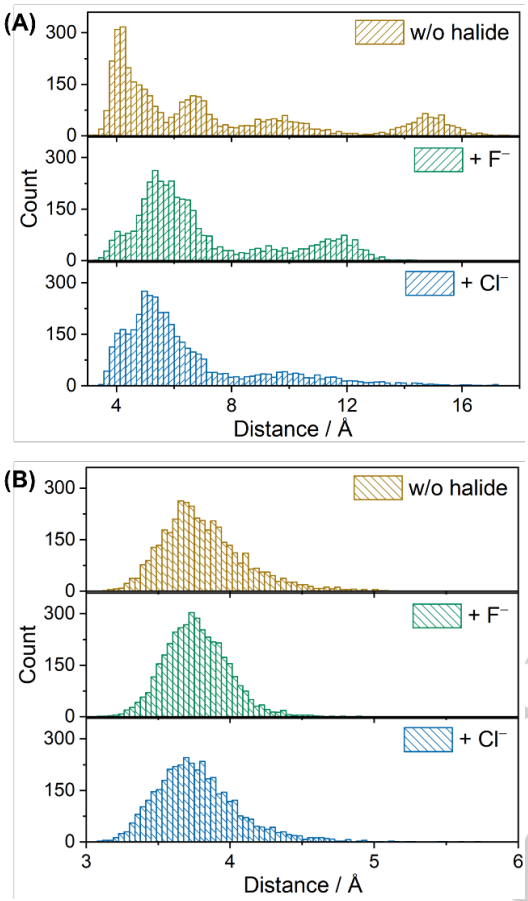

Figure 9. Distributions of the minimal ring-to-ring distance between FAD_{ox} and Tyr68 (A) and Tyr515 (B) in the MD simulations of halide-free GOX, as well as the simulations containing F^- or Cl^-.

These results are also reflected in the analysis of ΔRMSF, where the binding of halides, especially F^-, reduces the flexibility of Tyr68 and Tyr515 (Figure 7). The narrower distribution of the FAD_{ox}–Tyr68/Tyr515 distances with the maximum shifted towards longer distances (Figure 10) explains the more homogeneous excited-state decay (fitted with a single 7-ps phase) in F^- binding GOX. While the distance distribution overall is broader in halide-free GOX, the shortest distances between 3.0 to 3.5 Å are relatively more likely which allow the tyrosine electron donors to access positions closer to the flavin ring, facilitating the photoinduced ET reaction and thus resulting in a multiphasic but overall more efficient excited-state quenching (2 and 9 ps). In the GOX:Cl^- complex, the larger (therefore, more polarizable) Cl^-[43] and closer contact between Cl^- and the FAD_{ox} cofactor (Figure 6) can facilitate efficient orbital overlaps, supporting our proposal that substantial anion–π interactions exist between Cl^- and the aromatic flavin ring, which is absent or negligible in the GOX:F^- complexes. Such interactions within the GOX:Cl^- complex, although modest in the ground state, may significantly manifest in the excited state[44] and lead to the unprecedented ultrafast excited state decay in < 100 fs via an "intramolecular-like" CT excited state.[40] Hole-electron analysis[45] on the S_0 to S_1 transition of the flavin–chloride complex indeed exhibits CT characteristics, with the electron moving from Cl^- to FAD_{ox} (Figure S16).

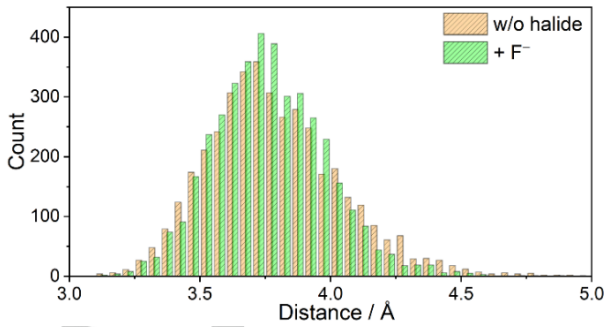

Figure 10. Distributions of the minimal ring-to-ring distances between FAD_{ox} and either one of the close-by tyrosines (Tyr68, Tyr515; see also Figure 9) in the MD simulations of halide-free GOX and the simulations containing F^-. Histograms are shown pairwise.

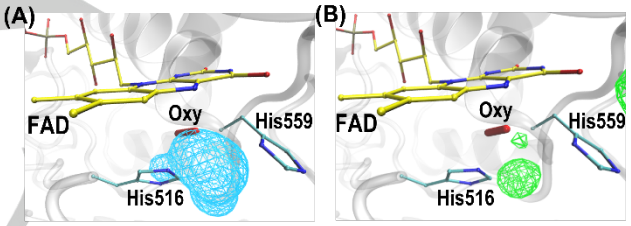

Figure 11. Comparison of the binding sites of Cl^- (A) and F^- (B) obtained from the MD simulations (see Figure 6) and the experimentally determined binding site of a molecular oxygen from the crystal structure of the F9 variant of GOX (PDB entry: 5NIW).[18] The structure of this variant is aligned to the backbone of the wild-type GOX (PDB entry: 1CF3), and only the structure of the wild-type GOX is shown for clarity.

Finally, we note that our results also provide direct evidence to support that Cl^- binds at a position close to the flavin *re*-face and between His516 and His559, as previously proposed by Jorns and coworkers,[9] which demonstrates that the active site of GOX is indeed capable of specific binding of anions, and therefore of stabilizing the $O_2^{\bullet-}$ intermediate during the oxygen activation process. MD simulations of GOX with O_2 or $O_2^{\bullet-}$ have been reported,[16] where a O_2 or $O_2^{\bullet-}$ molecule was placed in the active site of GOX, at a position close to His516, His559 and the flavin (the assumed oxygen activation site). The results show that only $O_2^{\bullet-}$ can be stabilized in this site while O_2 moves away, which is in general agreement with our findings. It is also worth noting that in our study at the beginning of our simulations we did not place the halides in the protein active site but randomly placed them in

the water box and it turned out that the halides indeed can diffuse into and be stabilized in the protein active site.

Recently, a crystal structure of a variant of GOX has been reported, where an electron density was found to be situated at a similar position, which was assigned to a molecule of oxygen.[18] Here, we compare the density maps of F^- and Cl^- in the active site of GOX obtained from the MD simulations with this experimentally determined oxygen binding site (Figure 11). We found the space with a significant density of Cl^- in our MD simulations overlapping well with the molecular oxygen site as demonstrated in Figure 11. Therefore, in GOX, Cl^- can be considered as a reasonable proxy for $O_2^{\bullet-}$ in structural and mechanistic studies, whereas F^- also occupies other binding sites. Moreover, occupation of the oxygen activation site and interactions with His516, the catalytic base in the oxidative and the reductive part of the catalytic cycle,[16] should be an important factor in the GOX inhibition by halides.[19] For the GOX:Cl^- complex, our results also strongly suggest the presence of CT interactions between the FAD_{ox} and Cl^-, which can affect the redox potential of GOX.[20] We speculate that this disfavors the ET reactions that are required in the catalytic cycle and contributes to the inhibition of GOX as well.

Conclusion

We have performed a comprehensive investigation of the F^-- and Cl^--binding properties of GOX by studying flavin-related photochemical processes. Combining ultrafast spectroscopic measurements and all-atom MD simulations, we revealed the intriguingly opposite effects of F^-- and Cl^--binding on the excited-state dynamics of the FAD_{ox} cofactor and the rationales behind the observations. We demonstrated that in GOX, Cl^- binding results in ultrafast quenching of the flavin fluorescence in < 100 fs, most likely via a CT-like excited state. The time-resolved dynamics as well as the transient spectrum of the product state that follows the CT excitation between FAD_{ox} and Cl^-, to the best of our knowledge, are documented here for the first time. By contrast, F^- binding leads to overall less efficient, but kinetically more homogeneous, fluorescence quenching, which is explained by the decrease of the flexibility of an important electron-donating residue, Tyr68, upon the F^- accommodation. By detailing the interactions of the halides with the active site of GOX, a well-characterized representative model system, this work provides a molecular basis of employing halides as mimics for anionic oxygen species in the structural and mechanistic study of flavoprotein oxidases.

In particular, our results help to understand the differences in the inhibitory effectiveness of F^- and Cl^- as observed in GOX:[17] F^- can bind to the protein more effectively, and primarily affects the reductive half-reaction of the catalytic cycle by increasing the active-site rigidity and locking the functionally important residue, His516, in a noncatalytic conformation. On the other hand, Cl^- interacts with the FAD_{ox} cofactor more closely, through anion–π interactions with a CT component, therewith influencing the redox properties of the cofactor. Moreover, Cl^- is more likely to have an impact on the oxidative half-reaction by specifically occupying the oxygen activation site, as demonstrated by the present MD simulations and the crystallographic structure of GOX containing O_2. Nevertheless, we did find that, although the effects are less profound, the Cl^- binding also increases the active-site rigidity of GOX, and a fraction of F^- can also bind the oxygen activation site. This suggests that the underlying mechanisms of the GOX inhibition by halides are very likely to have multiple contributors. As under acidic conditions concentrations of Cl^- required to completely inhibit GOX are on the order of those of typical physiological conditions (~100 mM), and under certain circumstances the presence of F^- can also be functionally relevant (e.g., in F^--containing pollutants), we anticipate that this work is relevant for applications of GOX as biocatalysts or biosensors.

Methods

Materials. GOX from *Aspergillus niger* was purchased from Sigma-Aldrich and used without further purification. Potassium citrate buffer (~50 mM) was used for all the measurements. Potassium chloride (KCl) and potassium fluoride (KF) were purchased from Sigma-Aldrich.

Steady-state spectral titrations. Protein samples were prepared with a flavin concentration of ~20 μM in 1-cm path length quartz cells at pH 3.0, 3.5 and 4.0, and titrated with concentrated salt solutions. Steady-state absorption and fluorescence emission spectra were recorded at room temperature using a Shimadzu UV−vis 1700 spectrometer and a Cary Eclipse fluorometer, respectively. Titrations were carried out at room temperature. Dissociation constants (K_d) for complexes formed with GOX at different pH were determined by fitting a theoretical binding curve:

$$\Delta A_{obs} = \frac{\Delta A_{max}[F^-]}{K_d + [F^-]} \qquad (1)$$

where ΔA_{obs} is the observed absorbance change at a given wavelength during the titration process, ΔA_{max} is the corresponding absorbance change corresponding to 100% complex formation and also a fitting parameter and $[F^-]$ is the concentration of F^- in the solution. In dilute aqueous solution hydrogen fluoride (HF) is a weak acid; when the protein concentration is much lower than the salt concentration in the solution, $[F^-]$ can be calculated by:

$$[F^-] = \frac{K_a[KF]}{K_a + [H^+]} \qquad (2)$$

where $[KF]$ is the concentration of KF added, corrected for dilution in the titration experiments, K_a is the acid dissociation constant of HF, with a value of 6.8×10^{-4},[46] and $[H^+]$ is the concentration of H^+ as given by the pH value.

To determine the free flavin content, the protein sample was washed with excess buffer and filtered with a 30-kDa cutoff Amicon Ultra 4 filter (Millipore). The filtrate was collected, and its UV-vis absorption spectrum was then measured.

Time-resolved spectroscopy. The setup for time-resolved fluorescence employing a Kerr gate was described previously.[24] Briefly, part of the 780 nm output from a Ti:sapphire laser/amplifier system (Quantronix Integra-C) operating at 0.5 kHz was passed through a BBO crystal, generating an excitation pulse centered at 390 nm. The remaining 780 nm beam was directed through a motorized delay line and focused into the Kerr medium where it spatially overlapped the fluorescence from the sample. The gated fluorescence was then detected with spectral resolution using a polychromator and a CCD camera configured as an array detector. Kerr media with different time-resolution/sensitivity compromises were used, i.e., suprasil (response time ~200 fs) and CS_2 (response time ~1 ps).

Multicolor time-resolved absorption spectra were recorded by the pump–probe technique on an instrument operating at 0.5 kHz, as described previously.[26] Pump pulses centered at 390 nm were obtained by second

harmonic generation of the fundamental beam, and continuum broadband pulses passed through a prism-compressor were used as the probe. Pump and probe beams were set at the magic angle (54.7°) to record the isotropic transient spectra. The excitation power was adapted such that each shot of the pump beam excited less than 10% of the sample. All the time-resolved experiments were conducted at the temperature of 10 ℃ and pH 3.0. The acidic pH was chosen because the enzyme is more active at acidic pH's , and at pH 3.0, it is completely inhibited by 100 mM KCl.[17] Global analysis of the data in terms of multi-exponential kinetics was performed using the Glotaran package.[47]

MD simulations with classical force fields. The structure of GOX from *Aspergillus niger* was taken from the Protein Data Bank (PDB entry: 1CF3; resolution: 1.9 Å).[41] The CHARMM36 force field was used for the protein residues [48] and the TIP3P model for water;[49] a recently developed force field for flavins was used to describe the FAD_{ox} cofactor.[50] Van der Waals parameters for F^- were taken from Ref. [51]. The protonation states of all titratable residues were assigned based on a PROPKA 3.1 analysis[52] and verified by ideal stereochemistry taking into account of steric effects and potential hydrogen-bonding interactions. In particular, to correspond to the low pH condition in the time-resolved experiments described above, required for efficient anion binding, titratable residues within 12 Å of the FAD binding site with pK_a's > 4.0 were protonated and both His516 and His559 were doubly protonated in MD simulations. The protonated oxygen in carboxylic acids was assigned based on ideal stereochemistry. A disulfide bridge was created between Cys164 and Cys206. The system was centered in a cubic box of aqueous solvent, at least 12 Å away from each of the box edges; the final system contained around 25,000 water molecules. To simulate the binding processes, 40 F^- or 40 Cl^-, which corresponds to ~100 mM, were randomly placed in the water box, and an appropriate number of K^+ was included to neutralize the net charge of the systems. MD simulations were performed using the NAMD program (version 2.13).[53] Periodic boundary conditions were assumed with long-range electrostatic interactions computed using the particle mesh Ewald method.[54] The integration time step was set at 2 fs. After energy minimization, the system was equilibrated first in an NVT ensemble for 50 ps, followed by a 500 ps simulation in the NPT ensemble, at 295 K and 1.0 atm pressure. The Berendsen thermostat and barostat were employed, with a relaxation time of 500 fs and four timesteps between position rescalings for constant pressure simulations.[55] The production runs were performed for 100 ns, collecting coordinates of the system every 100 ps. Four independent simulations were performed with randomly assigned initial positions of Cl^- or F^-, with the sampling time amounting to 400 ns in total for each halide. 400-ns MD simulations of the protein system in the absence of F^- and Cl^- were also carried out for comparison; this system was neutralized with 20 K^+. Density maps of Cl^- and F^- were generated with the VolMap tool of VMD 1.9.3.[56] Identified binding sites were further characterized by calculating the residence probability of ions by integrating the density within a sphere covering the binding site (a sphere radius of 4 Å was found to be appropriate).

QM-only and QM/MM calculations. To examine the effect of the spatial constraints of the protein active site on the complex stability, geometry optimization based on DFT of the flavin-halide complex outside the protein was performed at the B3LYP/def2-TZVP level[57,58] in implicit solvent. Moreover, to rationalize the effect of binding site charges on the absorption spectrum of FAD_{ox}, TDDFT calculations were performed at the B3LYP/def2-TZVP level. Excitation energies and oscillator strengths were calculated for 30 excited states and broadened using a Gaussian line shape with a full width at half height (FWHM) of 0.4 eV. The QM-only calculations were carried out using the ORCA package (version 4.0.1.2).[59], flavins were represented by a lumiflavin (the flavin chromophore), and the CPCM implicit solvent model[60] with a dielectric constant ε = 6 was used.[61] QM/MM-based geometry optimizations and TDDFT calculations were carried out using the pDynamo program (version 1.9.0)[62] coupled with the ORCA package. The QM and MM parts were described by DFT (B3LYP/6-31+G*) and the CHARMM force field, respectively. QM–MM electrostatic interaction were treated using the electrostatic embedding. The independent gradient model based on Hirshfeld partition of molecular density (IGMH)[63] was used to visualize Intermolecular interactions, and hole-electron analysis[45] was used to visualize the characteristics of the electronic transition, which were performed with Multiwfn program (version 3.8).[64] Further details concerning the setup of these QM and QM/MM calculations are given in the captions of Figure S8, S9, S10 and S16.

Acknowledgements

B.Z. thanks the China Scholarship Council for providing a Ph.D. scholarship.

Conflict of Interest

The authors declear no conflict of interest.

Data Availability Statement

The data that support the findings of this study are available from the corresponding authors upon reasonable request.

Keywords: Ab initio calculations • Flavoproteins • Halides • Molecular dynamics • Oxidoreductases • Ultrafast spectroscopy

[1] A. Mattevi, *Trends Biochem. Sci.* **2006**, *31*, 276–283.
[2] W. P. Dijkman, G. De Gonzalo, A. Mattevi, M. W. Fraaije, *Appl. Microbiol. Biotechnol.* **2013**, *97*, 5177–5188.
[3] V. Massey, *J. Biol. Chem.* **1994**, *269*, 22459–22462.
[4] E. Romero, J. R. Gómez Castellanos, G. Gadda, M. W. Fraaije, A. Mattevi, *Chem. Rev.* **2018**, *118*, 1742–1769.
[5] G. Gadda, *Biochemistry* **2012**, *51*, 2662–2669.
[6] J. P. Roth, J. P. Klinman, *Proc. Natl. Acad. Sci. USA* **2003**, *100*, 62–67.
[7] J. P. Klinman, *Acc. Chem. Res.* **2007**, *40*, 325–333.
[8] C. A. McDonald, R. L. Fagan, F. Collard, V. M. Monnier, B. A. Palfey, *J. Am. Chem. Soc.* **2011**, *133*, 16809–16811.
[9] P. R. Kommoju, Z. W. Chen, R. C. Bruckner, F. S. Mathews, M. S. Jorns, *Biochemistry* **2011**, *50*, 5521–5534.
[10] D. Roeser, B. Schmidt, A. Preusser-Kunze, M. G. Rudolph, *Acta Cryst.* **2007**, *63*, 621–627.
[11] N. Colloc'h, L. Gabison, G. Rald Monard, M. Altarsha, M. Chiadmi, G. Marassio, J. Sopkova-De, O. Santos, M. El Hajji, B. Castro, J. H. Abraini, T. Prangé, *Biophys. Journa* **2008**, *95*, 2415–2422.
[12] R. A. Steiner, H. J. Janssen, P. Roversi, A. J. Oakley, S. Fetzner, *Proc. Natl. Acad. Sci. U. S. A.* **2010**, *107*, 657–662.
[13] D. Zafred, B. Steiner, A. R. Teufelberger, A. Hromic, P. A. Karplus, C. J. Schofield, S. Wallner, P. Macheroux, *FEBS J.* **2015**, *282*, 3060–3074.
[14] E. Schuster, N. Dunn-Coleman, J. Frisvad, P. Van Dijck, *Appl. Microbiol. Biotechnol. 2002 594* **2002**, *59*, 426–435.
[15] S. B. Bankar, M. V. Bule, R. S. Singhal, L. Ananthanarayan, *Biotechnol. Adv.* **2009**, *27*, 489–501.
[16] V. Leskovac, S. Trivić, G. Wohlfahrt, J. Kandrač, D. Peričin, *Int. J. Biochem. Cell Biol.* **2005**, *37*, 731–750.
[17] M. K. Weibel, H. J. Bright, *J. Biol. Chem.* **1971**, *246*, 2734–2744.
[18] P. Dušan, D. Frank, S. Caroline, L. Kamerlin, K. Hoffmann, B.

Strodel, *ACS Catal.* **2017**, *7*, 6188−6197.

[19] M. J. Rogers, K. G. Brandtf, *Biochemistry* **1971**, *10*, 4630–4635.

[20] S. Vogt, M. Schneider, H. Schäfer-Eberwein, G. Nöll, *Anal. Chem.* **2014**, *86*, 7530–7535.

[21] N. Mataga, H. Chosrowjan, Y. Shibata, F. Tanaka, Y. Nishina, K. Shiga, *J. Phys. Chem. B* **2000**, *104*, 10667–10677.

[22] P. A. W. Van Den Berg, S. B. Mulrooney, B. Gobets, I. H. M. Van Stokkum, A. Van Hoek, C. H. Williams, A. J. W. G. Visser, *Protein Sci.* **2001**, *10*, 2037–2049.

[23] H. Staudt, D. Oesterhelt, M. Grininger, J. Wachtveitl, *J. Biol. Chem.* **2012**, *287*, 17637–17644.

[24] S. P. Laptenok, L. Bouzhir-Sima, J. C. Lambry, H. Myllykallio, U. Liebl, M. H. Vos, *Proc. Natl. Acad. Sci. U. S. A.* **2013**, *110*, 8924–8929.

[25] B. Zhuang, L. Nag, P. Sournia, A. Croitoru, R. Ramodiharilafy, J.-C. Lambry, H. Myllykallio, A. Aleksandrov, U. Liebl, M. H. Vos, *Photochem. Photobiol. Sci.* **2021**, *20*, 663–670.

[26] B. Zhuang, D. Seo, A. Aleksandrov, M. Vos, *J. Am. Chem. Soc.* **2021**, *143*, 2757–2768.

[27] N. Dozova, F. Lacombat, M. Lombard, D. Hamdane, P. Plaza, *Phys. Chem. Chem. Phys.* **2021**, *23*, 22692–22702.

[28] K. Sato, Y. Nishina, K. Shiga, *J. Biochem.* **1992**, *111*, 359–365.

[29] F. Neri, D. Kok, M. A. Miller, G. Smulevich, *Biochemistry* **1997**, *36*, 8947–8953.

[30] D. Arosio, G. Garau, F. Ricci, L. Marchetti, R. Bizzarri, R. Nifosì, F. Beltram, *Biophys. J.* **2007**, *93*, 232–244.

[31] Y. P. Yurenko, S. Bazzi, R. Marek, J. Kozelka, *Chem. - A Eur. J.* **2017**, *23*, 3246–3250.

[32] J. Kozelka, *Eur. Biophys. J.* **2017**, *46*, 729–737.

[33] D. Zhong, A. H. Zewail, *Proc. Natl. Acad. Sci. U.S.A.* **2001**, *98*, 11867–11872.

[34] A. Lukacs, R. K. Zhao, A. Haigney, R. Brust, G. M. Greetham, M. Towrie, P. J. Tonge, S. R. Meech, *J. Phys. Chem. B* **2012**, *116*, 5810–5818.

[35] L. Nag, A. Lukacs, M. H. Vos, *ChemPhysChem* **2019**, *20*, 1793–1798.

[36] P. F. Heelis, *Chem. Soc. Rev.* **1982**, *11*, 15–39.

[37] T. Sen, Y. Ma, I. V. Polyakov, B. L. Grigorenko, A. V. Nemukhin, A. I. Krylov, *J. Phys. Chem. B* **2021**, *125*, 757–770.

[38] S. Kepler, M. Zeller, S. V Rosokha, *J. Am. Chem. Soc* **2019**, *141*, 9338–9348.

[39] E. C. Breinlinger, C. J. Keenan, V. M. Rotello, *J. Am. Chem. Soc.* **1998**, *120*, 8606–8609.

[40] S. Hashimoto, R. Takagi, K. Okamura, A. Yabushita, T. Kobayashi, I. Iwakura, *Chem. Phys.* **2021**, *551*, 111326.

[41] G. Wohlfahrt, S. Witt, J. Hendle, D. Schomburg, H. M. Kalisz, H. J. Hecht, *Acta Crystallogr. Sect. D Biol. Crystallogr.* **1999**, *55*, 969–977.

[42] B. Zhuang, R. Ramodiharilafy, U. Liebl, A. Aleksandrov, M. H. Vos, *Proc. Natl. Acad. Sci.* **2022**, *119*, e2118924119.

[43] J. N. Wilson, R. M. Curtis, *J. Phys. Chem.* **1970**, *74*, 187–196.

[44] N. Hopkins, R. J. Stanley, *Biochemistry* **2003**, *42*, 991–999.

[45] Z. Liu, T. Lu, Q. Chen, *Carbon N. Y.* **2020**, *165*, 461–467.

[46] N. E. Vanderborgh, *Talanta* **1968**, *15*, 1009–1013.

[47] J. J. Snellenburg, S. P. Laptenok, R. Seger, K. M. Mullen, I. H. M. van Stokkum, *J. Stat. Softw.* **2012**, *49*.

[48] J. Huang, A. D. Mackerell, *J. Comput. Chem.* **2013**, *34*, 2135–2145.

[49] W. L. Jorgensen, J. Chandrasekhar, J. D. Madura, R. W. Impey, M. L. Klein, *J. Chem. Phys.* **1983**, *79*, 926–935.

[50] A. Aleksandrov, *J. Comp. Chem.* **2019**, *40*, 2834–2842.

[51] H. M. Senn, D. O'Hagan, W. Thiel, *J. Am. Chem. Soc.* **2005**, *127*, 13643–13655.

[52] M. H. M. Olsson, C. R. SØndergaard, M. Rostkowski, J. H. Jensen, *J. Chem. Theory Comput.* **2011**, *7*, 525–537.

[53] J. C. Phillips, R. Braun, W. Wang, J. Gumbart, E. Tajkhorshid, E. Villa, C. Chipot, R. D. Skeel, L. Kalé, K. Schulten, *J. Comput. Chem.* **2005**, *26*, 1781–1802.

[54] T. Darden, D. York, L. Pedersen, *J. Chem. Phys.* **1993**, *98*, 10089–10092.

[55] H. J. C. Berendsen, J. P. M. Postma, W. F. van Gunsteren, A. DiNola, J. R. Haak, *J. Chem. Phys.* **1998**, *81*, 3684.

[56] W. Humphrey, A. Dalke, K. Schulten, *J. Mol. Graph.* **1996**, *14*, 33–38.

[57] A. D. Becke, *J. Chem. Phys.* **1993**, *98*, 1372–1377.

[58] F. Weigend, R. Ahlrichs, *Phys. Chem. Chem. Phys.* **2005**, *7*, 3297–3305.

[59] F. Neese, *Wiley Interdiscip. Rev. Comput. Mol. Sci.* **2012**, *2*, 73–78.

[60] V. Barone, M. Cossi, *J. Phys. Chem. A* **1998**, *102*, 1995–2001.

[61] L. Li, C. Li, Z. Zhang, E. Alexov, *J. Chem. Theory Comput.* **2013**, *9*, 2126–2136.

[62] M. J. Field, *J. Chem. Theory Comput.* **2008**, *4*, 1151–1161.

[63] T. Lu, Q. Chen, *J. Comput. Chem.* **2022**, *43*, 539–555.

[64] T. Lu, F. Chen, *J. Comput. Chem.* **2012**, *33*, 580–592.

Entry for the Table of Contents

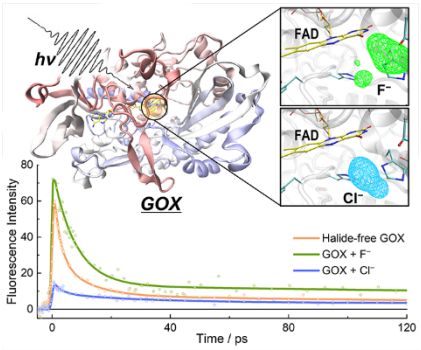

Compared with the halide-free GOX, Cl^- binding results in disappearance of fluorescence. By contrast, F^- binding leads to less efficient, and kinetically more homogeneous, fluorescence quenching. Such contrasting effects are rationalized by the differences in the binding behavior of F^- and Cl^- to the protein active site.

Institute and/or researcher Twitter usernames: @LabOptBio